Desalination and Water Treatment
www.deswater.com
doi: 10.5004/dwt.2019.24442

163 (2019) 125–132
September

Fabrication of Prussian blue/polydopamine layers on polyacrylonitrile membranes for efficient adsorption of cesium

Zhiqian Jia[a,*], Shuang Hao[a], Xiaoxue Cheng[a], Xiaoyu Lu[a], Lanying Tu[b]

[a]*Lab for Membrane Science and Technology, College of Chemistry, Beijing Normal University, Beijing 100875, China, emails: zhqjia@bnu.edu.cn (Z. Jia), sherily-Haos@bnu.edu.cn (S. Hao), xiaoxue @bnu.edu.cn (X. Cheng), xiaoyuLu @bnu.edu.cn (X. Lu)*
[b]*Department of Chemical Engineering, Qinghai University, Xining 810016, China, email: tulany1969@126.com*

Received 17 January 2019; Accepted 21 May 2019

ABSTRACT

Adsorption is an effective method for separating radioactive cesium (Cs^{137}) from solutions. Herein, polydopamine (PDA) film was fabricated on porous polyacrylonitrile (PAN) membranes, and then Prussian blue film was in-situ prepared on PDA. It was found for the first time that the PDA/PAN membrane showed good adsorption capacity for Cs^+ (0.074 mmol g^{-1}, 25°C) in mixed alkali metal ions solution with Cs^+/Li^+ selectivity of 7.5. The PB/PDA/PAN membranes displayed excellent adsorption performance for Cs^+ (0.498 mmol g^{-1}, 25°C) in mixed alkali metal ions solution with high selectivity (Cs^+/Li^+ = 42.3, Cs^+/Na^+ = 31.4, and Cs^+/K^+ = 18.4), as well as excellent stability even under ultrasonic conditions.

Keywords: Polydopamine; Prussian blue; Adsorption; In-situ preparation; Membrane; Cesium

1. Introduction

The treatment of radioactive wastes from nuclear plants is one of the challenging problems for mankind [1]. Cesium (Cs^{137}) is a fission product of nuclear fuels, and its removal from wastewater has attracted attentions due to its long half-life (30 years) [2]. Adsorption is an effective for separating cesium [3]. Grafted catechol resin, and resorcinol formaldehyde polycondensate resin are cheap adsorbents with relatively low Cs^+/Na^+ selectivity [4,5]. Zirconium tungstate, iron(III) hexacyanoferrate (Prussian blue, PB), etc. are ion-exchangers with high adsorption capacity and selectivity [6,7]. In our previous work [8], Prussian blue was in-situ prepared on porous polyacrylonitrile (PAN) membranes, and the membranes display high adsorption capacity due to the direct contact of PB layer with the solution. Nevertheless, the stability of PB layer on PAN membranes was not satisfactory.

Dopamine (DA) can self-polymerize and forms polydopamine (PDA) coating on most of materials [9–12], and can be applied for adhesion and surface immobilization [13]. As DA possessing catechol and amino groups, herein, we fabricated PDA on porous PAN membranes, and found good selectivity for cesium for the first time. Then, PB was prepared on the PDA film to further enhance the adsorption capacity and selectivity. PDA provided a platform for the growth of PB layer, resulting in excellent stability even under ultrasonic conditions.

2. Experimental

2.1. Materials

Analytical grade reagents of $K_4Fe(CN)_6$, $FeCl_3$, CsCl, RbCl, KCl, NaCl, LiCl, NH_4Cl and H_2SO_4 were employed. Dopamine (DA) and tris(hydroxymethyl)aminomethane (Tris) were provided by J&K Co. Ltd. PAN ultrafiltration membrane (MWCO 50,000) was bought from SEPRO Co. Ltd. The working solutions of alkali metal ions were prepared by

* Corresponding author.

stepwise dilution. DA solution (0.0105 mol L^{-1}) was prepared by dissolving DA (0.2 g) in Tris–HCl buffer solution (100 mL).

2.2. Methods

PAN membranes were put in 0.0105 mol L^{-1} of DA Tris-HCl solution (pH 8.5) at room temperature for a certain time, rinsed and then immersed in freshly prepared potassium ferrocyanide solution (0.025 mol L^{-1}) for 24 h. Then the membrane was rinsed and put in $FeCl_3$ solutions (0.005 and 0.025 mol L^{-1}, containing 0.01 mol L^{-1} hydrochloric acid) for 24 h [8,14].

2.3. Adsorption

The static adsorption was carried out in 50 mL of alkali metal solution under shaking at 25°C for 24 h. The adsorption capacity (Q_e, mmol g^{-1}) was expressed as:

$$Q_e = \frac{(C_0 - C_e) \times v_0}{w_0} \quad (1)$$

where C_0 and C_e are the initial and equilibrium metal ion concentration (mmol L^{-1}) respectively, v_0 is the solution volume (L), w_0 is the adsorbent mass (g). In the dynamic adsorption, the membranes (Φ50 mm) were first preconditioned with 3 × 5 mL of water, and then 100 mL of aqueous solution flowed through the membranes at a rate of 3.33 mL min^{-1}, and the filtrate was collected at a certain interval. In the dynamic desorption, a certain volume of eluting agent flowed through the membranes at a rate of 0.2 mL min^{-1} (0.03 MPa), and the eluent concentration was measured.

2.4. Characterization

The morphologies of membranes were observed with a field emission scanning electron microscope (FESEM, Hitachi S-4800, Japan). The IR spectra were measured by Fourier transform infrared spectrophotometer (FTIR, Affinity-1, Shimadzu, Japan). Powder XRD pattern was analyzed with monochromatized Cu Kα incident radiation (Shimadzu XRD-6000). The alkali metal concentrations were determined by inductively coupled plasma mass spectrometry (ICP-MS, NexION300x, PerkinElmer Instruments Co. Ltd.).

3. Results and discussion

3.1. PDA/PAN membranes

In the preparation of PDA/PAN membranes, the PAN membrane was immersed in DA Tris-HCl solution (pH 8.5) at room temperature for a certain time. The polymerization of DA includes two mechanisms [15]: oxidation of catechol to dopaquinone, followed by reverse dismutation reaction of DA with dopaquinone, and cross-linking polymerization; Intramolecular cyclization of DA, and then oxidation, rearrangement and cross-linking. With the increased polymerization time (1, 3, 6, 9 and 12 h), the color of PAN membranes changed from white to yellow and brown, and the PDA mass fraction (in term of PAN membranes) rose from 0.28% to 0.36%, 0.45%, 0.52% and 0.57%, and the PDA thickness increased from 0.1 (6 h) to 0.4 μm (9 h) and 2.0 μm (12 h) while the membrane pores size decreased (Fig. 1). Meanwhile, the adsorption capacity for Cs^+ in 1 mmol L^{-1} of CsCl solution (25 mL, 25°C) rose (Fig. 2a), while the permeation fluxes in vacuum filtration declined (8.22, 7.89, 7.10, 6.15, 5.45 and 3.10 mL min^{-1}) (Fig. 2b). Considering the permeation fluxes and adsorption capacity, 9 h was employed for DA polymerization.

The effects of pH values of Cs^+ solution on the adsorption performance of PDA/PAN membranes were given in Fig. 2c. The adsorption capacity increased with pH values (4, 5, 6, 7 and 8) due to the competition of H^+ with Cs^+ for the adsorption sites at acidic conditions. Hereafter, pH 7 was employed for the adsorption. Fig. 2d gives the adsorption capacity of PDA layer for mixed alkali metal ions solution (1 mmol L^{-1} for Li^+, Na^+, K^+, Ru^+ and Cs^+ respectively, 50 mL, pH 7, and 25°C). It could be seen that the adsorption capacity was in the order of $Cs^+ > Rb^+ > K^+ > Na^+ > Li^+$, and the adsorption capacity for Rb^+ and Cs^+ attained to 0.067 and 0.074 mmol g^{-1} respectively. The selectivity factor of Cs^+ vs. Li^+, Na^+ and K^+ was 7.5, 3.61 and 2.54 respectively, demonstrating the high selectivity of PDA for Cs^+ and Rb^+. To our best knowledge, this is the first report about the selective adsorption of Cs^+ and Rb^+ by PDA. The static adsorption isotherm of PDA/PAN membranes for single CsCl solution was measured in 50 mL of Cs^+ solution (0.0075, 0.015, 0.038, 0.075, 0.15, 0.6 and 0.75 mmol L^{-1}) at pH 7 and 25°C. Fig. 2e shows that the adsorption capacity of PDA layer increased and then approached a maximum value (0.082 mmol g^{-1}, i.e. 10.9 mg g^{-1}). The Langmuir adsorption model provided a more satisfactory fitting (R^2 = 0.999) than the Freundlich model (Figs. 2f and g), demonstrating a chemical adsorption mechanism.

PDA possesses catechol groups, and the extraction of Cs^+ involves the cation exchange with a phenolic proton, R–OH + Cs^+ → R–OCs + H^+. Fig. 2h shows the pH evolution in adsorption of 100 mL of Cs^+ solutions (0.1 and 0.5 mmol L^{-1}). For 0.1 mmol L^{-1} of Cs^+ solution, the pH reduced from 6.48 to 6.29 after adsorption, and for 0.5 mmol L^{-1} Cs^+ solution the pH decreased from 6.48 to 6.25. The H^+ released was 1.82×10^{-8} mol and 2.3×10^{-8} mol respectively, which were comparable with that of Cs^+ adsorbed on PDA/PAN membranes (3.4×10^{-8} mol, 4.8×10^{-8} mol), confirming the cation exchange mechanism.

In IR spectra of PDA/PAN membranes (Fig. 3a), 2,242 cm^{-1} was ascribed to the C–N vibration of PAN membranes, and N–H vibration (1,510 cm^{-1}) and C=C (benzene ring) vibration (1,610 cm^{-1}) appeared after polymerization of DA, confirming the formation of PDA [16]. After adsorption of Cs^+, the –OH absorption (at 3,346 cm^{-1}) of PDA/PAN membranes significantly weakened. In the XPS full spectra of PDA/PAN membranes (Fig. 3b), the Cs 3d peak (734.1 eV) appeared after adsorption of Cs^+. The XPS peak fitting analysis of the O1s was shown in Figs. 3c and d. After adsorption of Cs^+, the peak area of C=O (531.2 eV) remained almost unchanged, while the peak area of OH (531.5 eV) decreased from 50.9% to 40.0%, and O–Cs peak appeared at 529.7 eV [17]. In EDS and mapping analyses of PDA/PAN membranes (Figs. 3e and f), the Cs elements appeared after adsorption of Cs^+. The selective adsorption of Cs^+ by PDA/PAN membranes is attributed to two reasons: The small

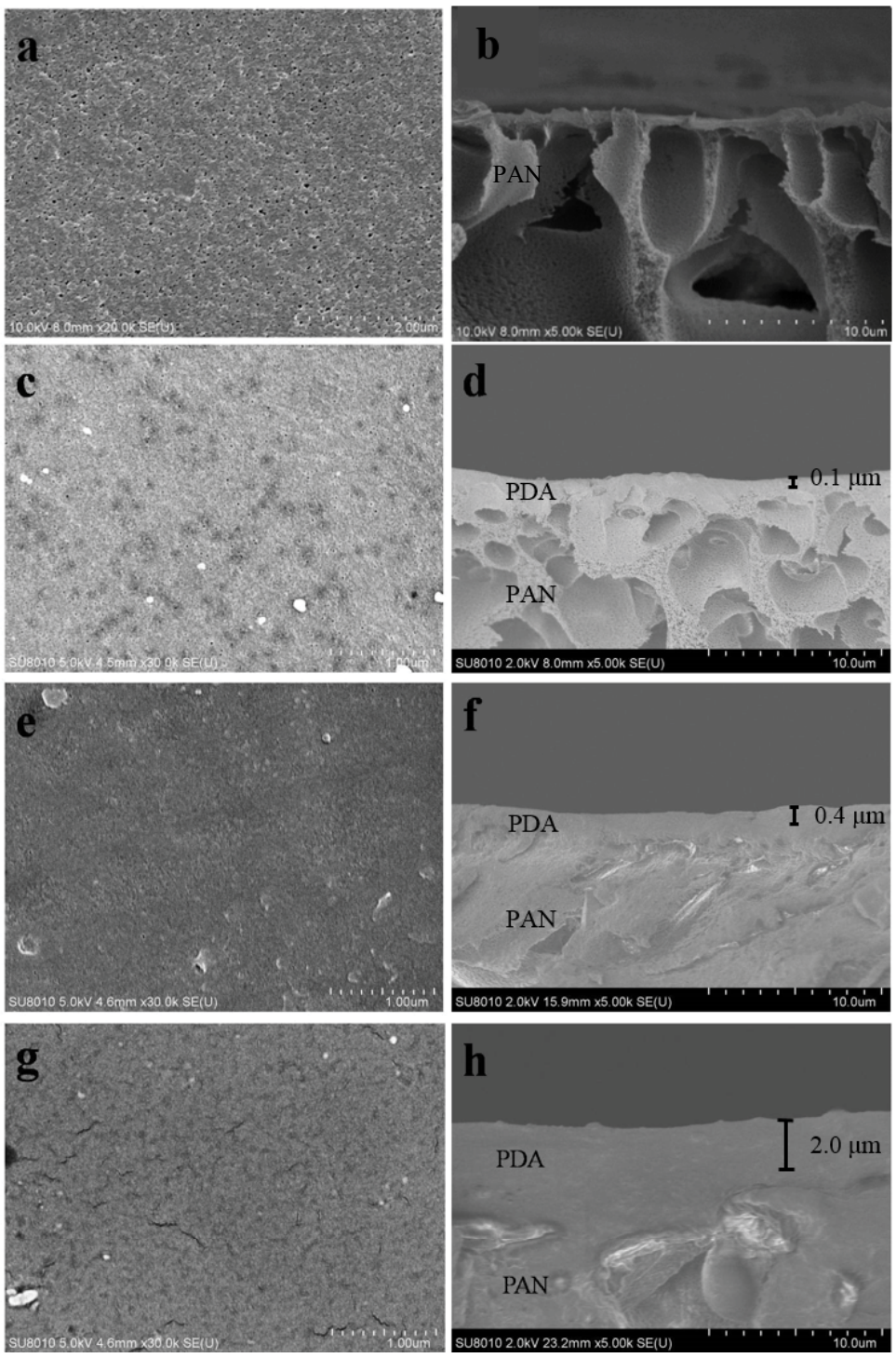

Fig. 1. SEM images of surface and cross-section of pristine PAN membranes (a, b), and PDA/PAN membranes grown for 6 h (c, d), 9 h (e, f), and 12 h (g, h).

hydration energy which needs to overcome when hydrated Cs^+ interacts with the hydroxyl groups of PDA [18]; the high stabilization of Cs^+-phenolate complex because of the strong interaction of weakly hydrated Cs^+ ions with the phenolate [19]. Therefore, the adsorption is dominated by hydration effects in solution, following the lyotropic series of $Cs^+ > Rb^+ > K^+ > Na^+ > Li^+$.

3.2. PB/PDA/PAN membranes

To further enhance the adsorption capacity and selectivity of membranes, Prussian blue layer was in-situ prepared on PDA/PAN membranes. The process includes the nucleation of PB on PDA/PAN in potassium ferrocyanide solution [20], and then growth in $FeCl_3$ solutions (0.005 and 0.025 mol L^{-1}),

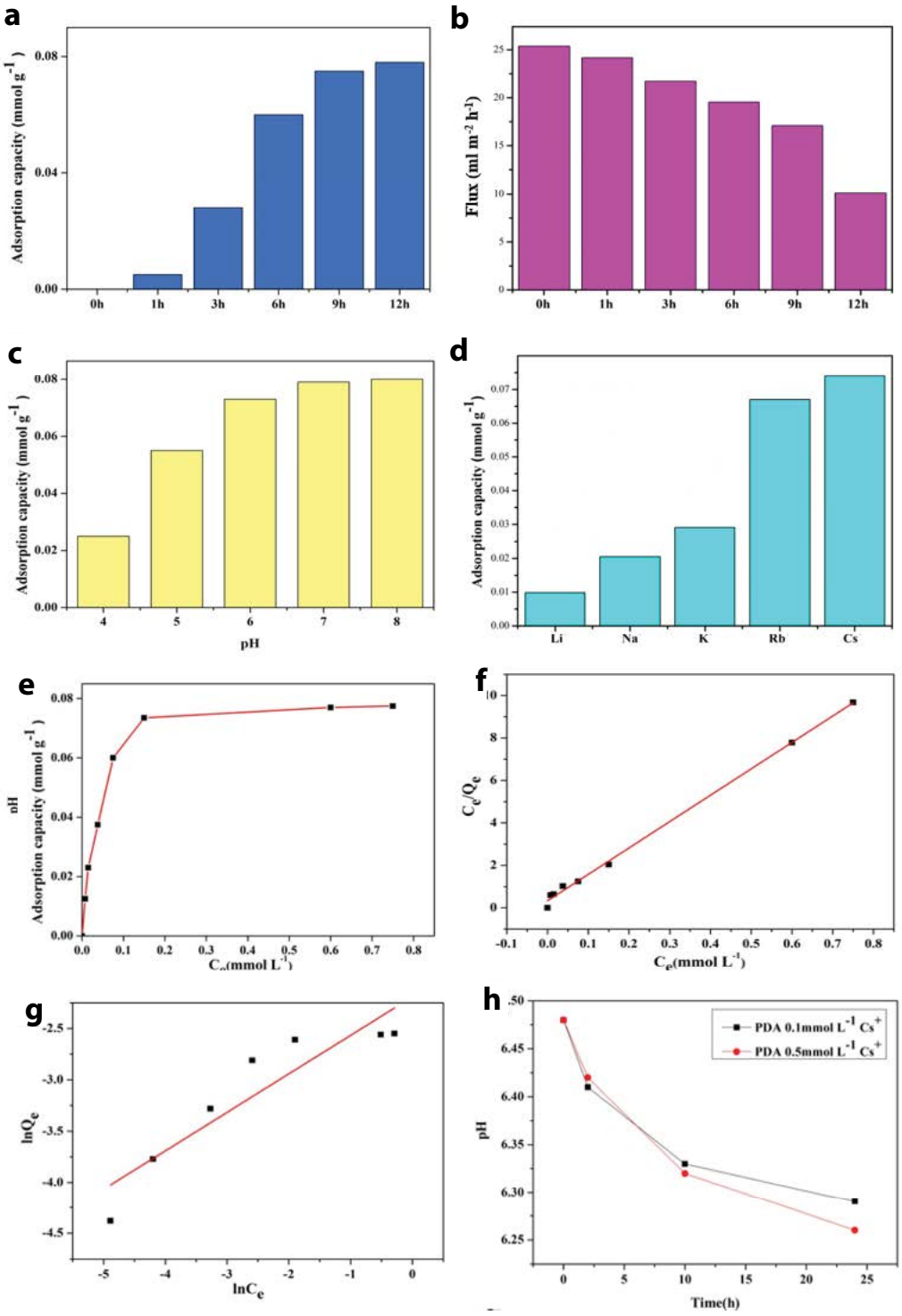

Fig. 2. PDA/PAN membranes. (a) Effects of polymerization time on adsorption capacity for Cs^+. (b) Effects of polymerization time on permeation fluxes. (c) Effects of pH on adsorption capacity of Cs^+. (d) Adsorption capacity for alkali metal ions. (e) Adsorption isotherm of Cs^+. (f) Linear fitted curve of Langmuir model. (g) Linear fitted curve of Freundlich model. (h) pH evolution in adsorption of Cs^+.

and the membrane color changed from brown to blue. The mass fraction of PB layer was found to be 0.23% and 0.49% of PAN membranes, and the thickness of PB layer was 0.5 and 1 μm, and the PB nanoparticles size was 100 and 60 nm (Fig. 4). The FTIR spectra (Fig. 3a) and XRD patterns of PB layer (Fig. 5) were consistent with the literature [21,22], confirming the formation of PB (fcc phase, space group of Fm3m).

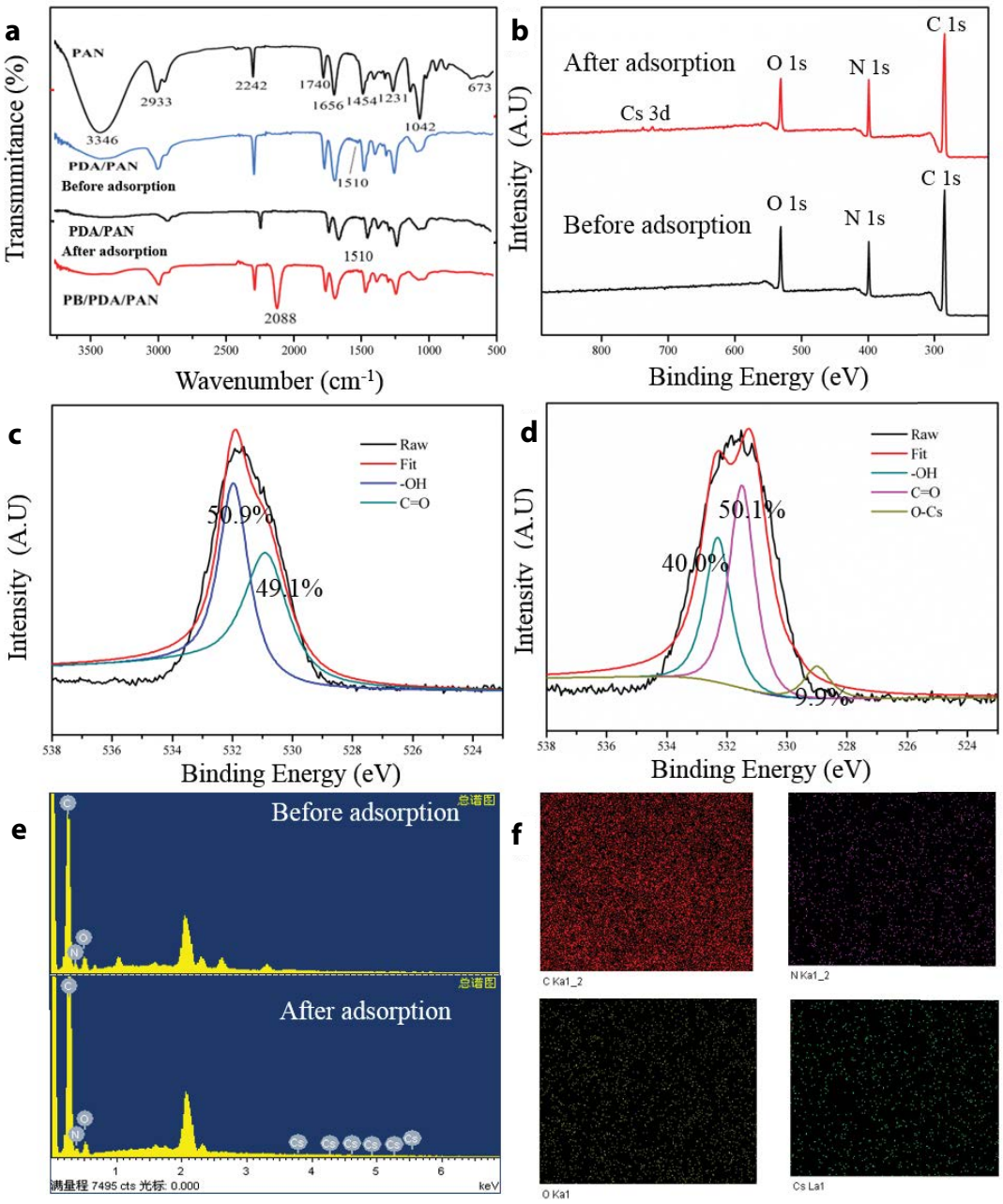

Fig. 3. Characterization of membranes. (a) FTIR spectra. (b) XPS spectra of PDA/PAN membranes before and after adsorption of Cs^+. (c) O1s XPS spectra before adsorption. (d) O1s XPS spectra after adsorption of Cs^+. (e) EDS spectra before and after adsorption of Cs^+. (f) Mapping after adsorption of Cs^+.

The adsorption of PB/PDA/PAN membranes for mixed alkali metal ions (50 mL, 1 mmol L^{-1} for every metal ion) was evaluated at pH 7 and 25°C. Fig. 6a shows that the adsorption capacity of PB/PDA layer for Cs^+ and Rb^+ were 0.498 and 0.421 mmol g^{-1}, and the ideal selectivity of Cs^+ vs. Li^+, Na^+, and K^+ was 42.3, 31.4, and 18.4 respectively. PB possesses a lot of lattice defect sites (vacant sites of $Fe(CN)_6^{4-}$), in which coordination and crystal H_2O molecules occupy. The hydrophilic spaces prefer to adsorb hydrated alkali metal ions. The radii of hydrated Cs^+ (0.329 nm) and Rb^+ (0.329 nm) are smaller than that of K^+ (0.331 nm), Na^+ (0.358 nm), and Li^+ (0.382 nm) [23]. The smaller radius of Cs^+ probably fits in PB lattice, and thus the PB/PDA/PAN membranes display size-sieving effects. It should be noted that, some literature discussed the ions radii using the Stokes radii [24]. As the Stokes radius is usually applied to gas bubbles and colloidal particles that are much larger than the solvent molecules, the concept of Stokes radius for ions is devoid of physical meaning [25]. When a Cs^+ ion occupies these hydrophilic spaces, a proton can be eliminated from the coordination water of Fe(III).

$$Fe^{III} - OH_2 + Cs^+ \rightarrow Fe^{III} - OH^- Cs^+ + H^+ \quad (2)$$

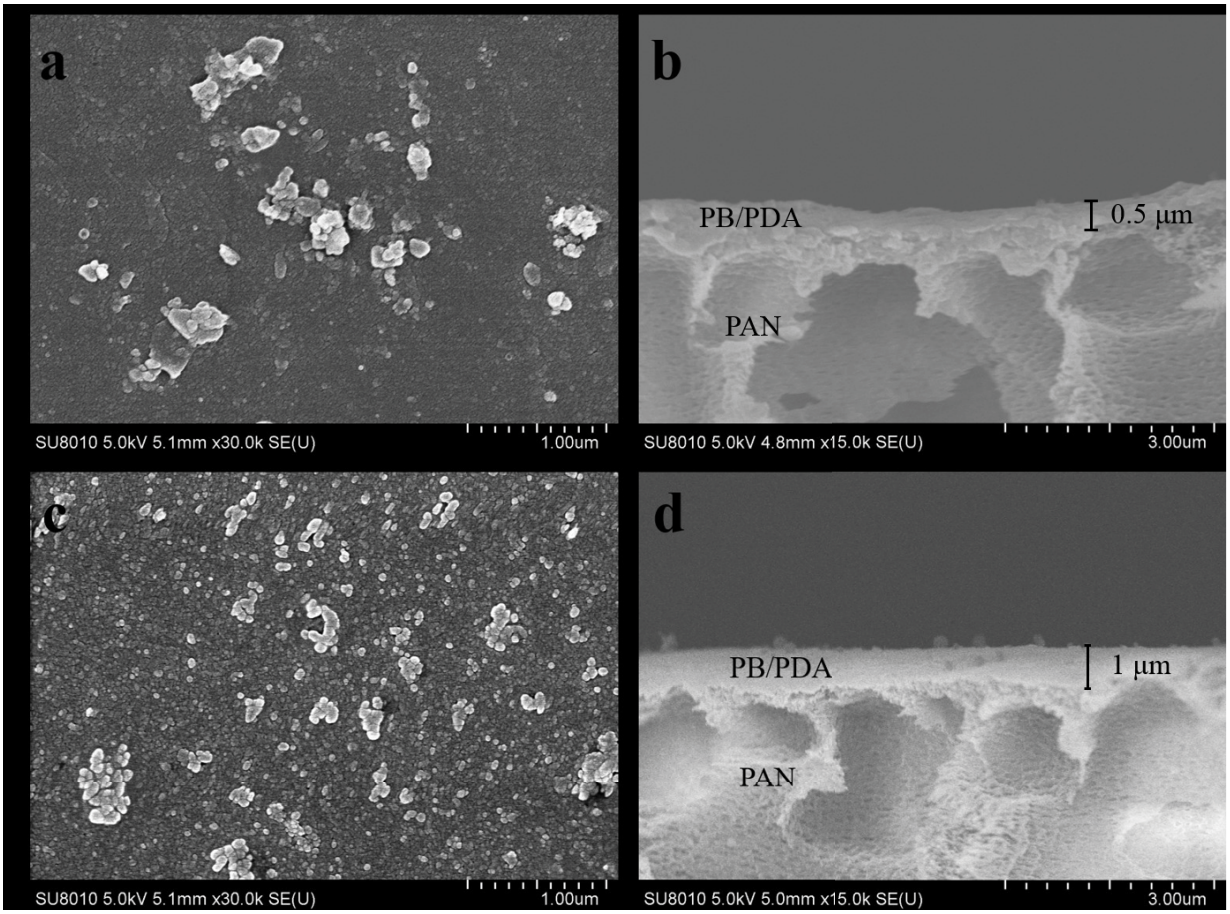

Fig. 4. SEM images of surface and cross-section of PB/PDA/PAN membranes. (a, b) 0.005 mol L^{-1} of $FeCl_3$ solution. (c, d) 0.025 mol L^{-1} of $FeCl_3$ solution.

Fig. 6b shows the pH evolution in the adsorption of 100 mL Cs^+ solutions (0.1 and 0.5 mmol L^{-1}). The pH reduces from 6.24 to 5.1 for 0.1 mmol L^{-1} Cs^+ solution and from 6.26 to 4.86 for 0.5 mmol L^{-1} Cs^+ solution, and the H^+ released is 7.36×10^{-7} mol and 1.33×10^{-6} mol respectively. These values were comparable with those of Cs^+ adsorbed on membranes (1.1×10^{-6} mol and 2.4×10^{-6} mol), partially demonstrating the proton-elimination mechanism. The static adsorption isotherm of PB/PDA/PAN membranes for single CsCl solution at 25°C was given in Fig. 6c. The maximum adsorption capacity of PB/PDA layer reached 0.514 mmol g^{-1} (68.4 mg g^{-1}), which was comparable with that of PB powder [26].

Fig. 6f gives the breakthrough curve in dynamic adsorption of CsCl solution (0.06 mmol L^{-1}, flow rate of 3.33 mL min^{-1}, 0.03 MPa). C/C_0 = 0.1 is defined as the breakthrough point, and C/C_0 = 0.8 as the saturation point, and the corresponding volume is defined as v_b and v_s, respectively. For PB/PDA/PAN membranes, v_b was 2.7 mL and v_s was 29.1 mL, and the saturation dynamic adsorption capacity is 0.143 mmol g^{-1} [14]. The saturated membranes was eluted with 10 mL of 0.1 mol L^{-1} NH_4Cl solution (containing 0.01 mol L^{-1} HCl) at a flow rate of 0.5 mL min^{-1}, and then reused in adsorption. Fig. 6e shows that there was no apparent decrease in adsorption capacity in the four adsorption/elution cycles, indicating the good reusability of membranes.

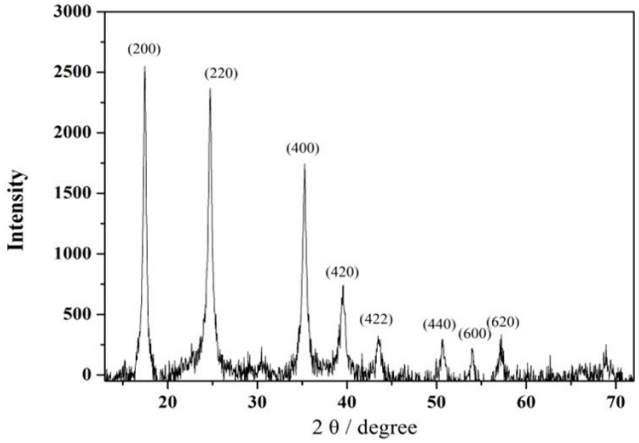

Fig. 5. Powder XRD of PB layer.

The stability of the PB/PDA/PAN membranes was evaluated under ultrasonic conditions. The PB/PDA/PAN membranes were ultrasonicated in an ultrasonic cleaner (100 w) for various times, and the mass loss was measured. For comparison, the mass loss of the PB/PAN membranes (i.e., growing PB directly on PAN membranes) was also

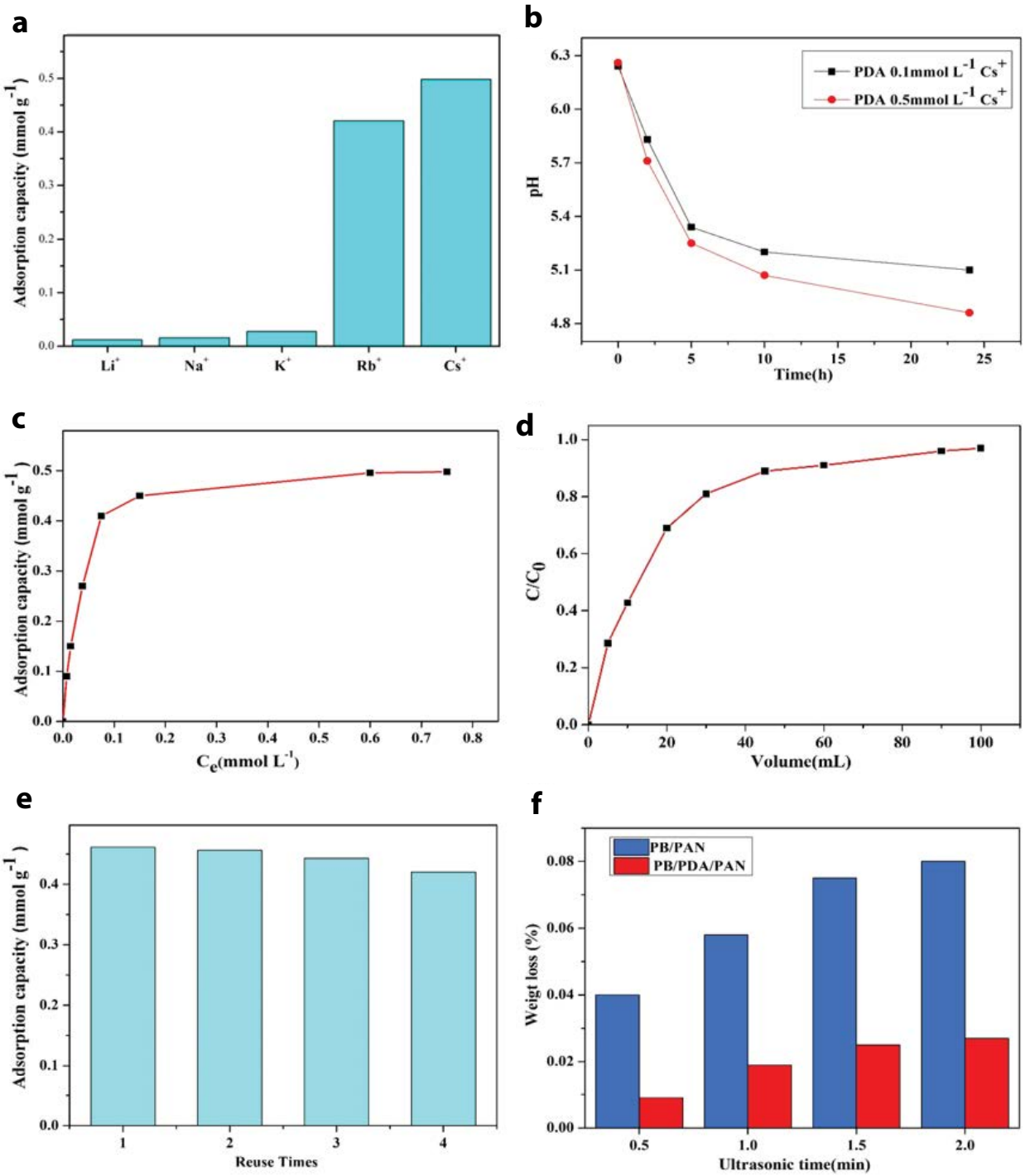

Fig. 6. PB/PDA/PAN membranes. (a) Adsorption capacity. (b) pH evolution in adsorption of Cs^+. (c) Adsorption isotherm of Cs^+. (d) Linear fitted curve of Langmuir model. (e) Reuse of PB/PDA/PAN membranes. (f) Membranes stability under ultrasonication.

determined. With the increased ultrasonic time (0.5, 1.0, 1.5 and 2.0 min), the mass loss of PB/PDA/PAN and PB/PAN membranes rose (Fig. 6f). At the same ultrasonic time, the mass loss of PB/PDA/PAN membranes was only about 20%–30% of that of the PB/PAN membranes, demonstrating the excellent stability of PB/PDA/PAN membranes even under extreme conditions.

4. Conclusions

PDA layer was facilely fabricated on PAN membranes, and displayed high adsorption capacity for Cs^+ (0.074 mmol g^{-1}) and selectivity (Cs^+/Li^+ = 7.5, Cs^+/Na^+ = 3.61) in mixed alkali metal ion solution. The adsorption capacity of PB/PDA layer for Cs^+ in the mixed metal ions solution attained to

0.498 mmol g^{-1}, and the selectivity of Cs^+ vs. Li^+, Na^+, and K^+ was 42.3, 31.4, and 18.4 respectively. The adsorption isotherm could be well described by the Langmuir adsorption model. The PB/PDA/PAN membranes displayed excellent stability even under ultrasonic conditions, indicating practical perspective for cesium adsorption.

Acknowledgements

This work was supported by the National Natural Science Foundation of China and Qinghai Qaidam Saline Lake Chemical Science Research Joint Fund (No. U1607109), and the State Key Laboratory of Chemical Resource Engineering (CRE-2016-C-305).

References

[1] P. Spezzano, Distribution of pre- and post-Chernobyl radiocaesium with particle size fractions of soils, J. Environ. Radioact., 83 (2005) 117–127.
[2] K.O. Buesseler, S.R. Jayne, N.S. Fisher, I.I. Rypina, H. Baumann, Z. Baumann, C.F. Breier, E.M. Douglass, J. George, A.M. Macdonald, H. Miyamoto, J. Nishikawa, S.M. Pike, S. Yoshida, Fukushima-derived radionuclides in the ocean and biota off Japan, Proc. Natl. Acad. Sci. U.S.A., 109 (2012) 5984–5988.
[3] T. Sangvanich, V. Sukwarotwat, R.J. Wiacek, R.M. Grudzien, G.E. Fryxell, R.S. Addleman, C. Timchalk, W. Yantasee, Selective capture of cesium and thallium from natural waters and simulated wastes with copper ferrocyanide functionalized mesoporous silica, J. Hazard. Mater., 182 (2010) 225–231.
[4] L.V. Tendeloo, B. de Blochouse, D. Dom, J. Vancluysen, R. Snellings, J.A. Martens, C.E.A. Kirschhock, A. Maes, E. Breynaert, Cation exchange properties of zeolites in hyper alkaline aqueous media, Environ. Sci. Technol., 49 (2015) 1729–1737.
[5] E.H. Borai, R. Harjula, L. Malinen, A. Paajanen, Efficient removal of cesium from low-level radioactive liquid waste using natural and impregnated zeolite minerals, J. Hazard. Mater., 172 (2009) 416–422.
[6] H. Mimura, H. Ohta, K. Akiba, Y. Onodera, Uptake behavior of americium on alginic acid and alginate polymer gels, J. Radioanal. Nucl. Chem., 247 (2001) 33–38.
[7] M.F. Attallah, E.H. Borai, Risto, Hariula, Airi, Paajanen, Mikko, Karesoja, Selective removal of cesium using zirconium (IV) tungstate as an inorganic ion exchanger from aqueous solution, Mater. Eng. B, 1 (2011) 736–746.
[8] Z. Jia, X. Cheng, Y. Guo, L. Tu, In-situ preparation of iron(III) hexacyanoferrate nano-layer on polyacrylonitrile membranes for cesium adsorption from aqueous solutions, Chem. Eng. J., 325 (2017) 513–520.
[9] X. Zhang, S. Wang, L. Xu, L. Feng, Y. Ji, L. Tao, S. Li, Y. Wei, Biocompatible polydopamine fluorescent organic nanoparticles: facile preparation and cell imaging, Nanoscale, 4 (2012) 5581–5584.
[10] Z.L. Rao, S. Liu, R. Wu, G. Wang, Z. Sun, L. Bai, W. Wang, H. Chen, H. Yang, D. Wei, Y. Niu, Fabrication of dual network self-healing alginate/guar gum hydrogels based on polydopamine-type microcapsules from mesoporous silica nanoparticles, Int. J. Biol. Macromol., 129 (2019) 916–926.
[11] S. Liu, Z. Rao, R. Wu, Z. Sun, Z. Yuan, L. Bai, W. Wang, H. Yang, H. Chen, Fabrication of microcapsules by the combination of biomass porous carbon and polydopamine for dual self-healing hydrogels, J. Agric. Food. Chem., 67 (2019) 1061–1071.
[12] Y. Liu, K. Ai, L. Lu, Polydopamine and its derivative materials: synthesis and promising applications in energy, environmental, and biomedical fields, Chem. Rev., 114 (2014) 5057–5115.
[13] K. Sun, Y. Xie, D. Ye, Y. Zhao, Y. Cui, F. Long, W. Zhang, X. Jiang, Mussel-inspired anchoring for patterning cells using polydopamine, Langmuir, 28 (2012) 2131–2136.
[14] Z. Jia, M. Jiang, G. Wu, Amino-MIL-53(Al) sandwich-structure membranes for adsorption of p-nitrophenol from aqueous solutions, Chem. Eng. J., 307 (2017) 283–290.
[15] X. Du, L. Li, J. Li, C. Yang, N. Frenkel, A. Welle, S. Heissler, A. Nefedov, M. Grunze, P.A. Levkin, UV-triggered dopamine polymerization: control of polymerization, surface coating, and photopatterning, Adv. Mater., 26 (2014) 8029–8033.
[16] L. Yang, J. Kong, D. Zhou, J.M. Ang, S.L. Phua, W.A. Yee, H. Liu, Y. Huang, X. Lu, Transition-metal-ion-mediated polymerization of dopamine: mussel-inspired approach for the facile synthesis of robust transition-metal nanoparticle-graphene hybrids, Chemistry, 20 (2014) 7776–7783.
[17] Q. Fang, B. Chen, Adsorption of perchlorate onto raw and oxidized carbon nanotubes in aqueous solution, Carbon, 50 (2012) 2209–2219.
[18] S.K. Samanta, B.M. Misra, Ion exchange selectivity of a resorcinol-formaldehyde polycondensate resin for cesium in relation to other alkali metal ions, Solvent Extr. Ion Exch., 13 (1995) 575–589.
[19] A. Favre-Réguillon, B. Dunjic, M. Lemaire, R. Chomel, Synthesis and evaluation of resorcinol-based ion-exchange resins for the selective removal of cesium, Solvent Extr. Ion Exch., 19 (2001) 181–191.
[20] Z. Jia, G. Sun, Preparation of prussian blue nanoparticles with single precursor, Colloids Surf., A, 302 (2007) 326–329.
[21] B. Haghighi, S. Varma, F.M. Alizadeh Sh, Y. Yigzaw, L. Gorton, Prussian blue modified glassy carbon electrodes—study on operational stability and its application as a sucrose biosensor, Talanta, 64 (2004) 3–12.
[22] F. Herren, P. Fischer, A. Ludi, W. Haelg, Neutron diffraction study of Prussian Blue, $Fe_4[Fe(CN)_6]_{3.3}H_2O$. Location of water molecules and long-range magnetic order, Cheminform, 19 (1980) 956–959.
[23] A.N. Romanov, F.V. Grigoriev, V.B. Sulimov, Estimation of Bi+ monocation crystal ionic radius by quantum chemical simulation, Comput. Theor. Chem., 1017 (2013) 159–161.
[24] E.R. Nightingale, Phenomenological theory of ion solvation. Effective Radii of hydrated ions, Biochim. Biophys. Acta, 63 (1958) 566–567.
[25] Y. Marcus, Are ionic stokes radii of any use?, J. Solution Chem., 41 (2012) 2082–2090.
[26] S.S. Madaeni, E. Salehi, A new adsorption–transport and porosity combined model for passage of cations through nanofiltration membrane, J. Membr. Sci., 333 (2009) 100–109.